

# Nucleation preexponential in dynamic Ising models at moderately strong fields

Vitaly A. Shneidman and Gelu M. Nita

*Department of Physics, New Jersey Institute of Technology, Newark, New Jersey 07102, USA*

(Received 23 February 2003; published 15 August 2003)

A dynamic Ising model on a two-dimensional square lattice with nearest neighbor interactions is considered in the metastable region at low temperatures. A large number of low-energy cluster configurations is identified, and for those configurations a system of kinetic equations is written. Solution is obtained using symbolic computational approaches. This allows one to identify the full expression for the nucleation rate, including the preexponential. The treatment generalizes the earlier study of a different, lattice-gas spin-flip dynamics [V. A. Shneidman and G. M. Nita, *Phys. Rev. Lett.* **89**, 025701 (2002)], for the cases of Glauber and Metropolis dynamics and for a broader region of fields. In addition, connection with the lowest-energy nucleation paths (which can be studied analytically, without computer assistance) is examined.

DOI: 10.1103/PhysRevE.68.021605

PACS number(s): 64.60.Qb, 05.50.+q, 05.40.-a, 02.50.Ga

## I. INTRODUCTION

The nucleation problem is ubiquitous in physics of metastable systems, including vapors [1], glass-forming liquids [2], glasses [3], thin solid films [4], electron-hole liquid [5], micromagnetic materials [6], or colloid systems [7] to name just a few.

In the early paper [8], Volmer and Weber identified the exponential part of the nucleation rate

$$I \propto \exp\left\{-\frac{W_*}{T}\right\}, \quad (1)$$

where  $T$  is the temperature (Boltzmann constant is taken as 1) and  $W_*$  is the minimal work required to form a critical nucleus. The value of  $W_*$  is infinite at phase equilibrium, but decreases upon intrusion into the metastable region, and in typical experiments nucleation is observed for  $W_*$  of the order of several tens of  $T$ . The latter conditions determines similarities of nucleation in systems of very different nature, and often Eq. (1) works rather accurately when predicting the dependence of the nucleation rate on supersaturation, which characterizes the deviation from equilibrium.

The situation is more subtle with respect to the preexponential (prefactor) in Eq. (1), which is sensitive to kinetics of a specific system. In terms of vapor condensation, Farkas and later Becker and Döring [8] suggested to treat nucleation as a random walk in the one-dimensional space of cluster sizes. Within this model (known today as *classical*), the nucleation rate can be obtained exactly, including the preexponential term. In the context of cavitation problem, Zeldovich further showed that even without specifying the microscopic detail of the nucleation process, the kinetic part of the preexponential can be extracted from macroscopic (hydrodynamic) equations which describe growth or decay of a single nucleus.

The conventional wisdom derived from early nucleation studies was that the preexponential only weakly depends on the supersaturation, approximately as a power law when phase equilibrium is approached. In practice, when scatter in the measured values of  $I$  can be within an order of magnitude, it can be exceptionally hard to distinguish the preexpo-

ponential on the background of the rapidly changing exponential term. The inevitable minor inaccuracies in  $W_*$  (usually due to uncertainties in the interfacial tension) can further complicate the task. At the same time, having a flexible fitting parameter in the nucleation rate makes it very hard to confirm (or rule out) a given theory. The “Lothe-Pound paradox” in vapor condensation [9,10] is one of the examples of the extreme span of opinions on the issue of the preexponential.

One hopes to get an additional insight from studies of model systems, such as the Ising model in nonzero field, where  $W_*$  can be derived exactly and where more controlled “measurements” (or predictions) of  $I$  compared to real-life experiments can be expected. In the high-temperature region, Fisher [11] (close to  $T_c$ ) and Langer [12] (away from  $T_c$ ) suggested nonclassical preexponentials for the nucleation rate. The nucleus here is isotropic and  $W_*$  for a given supersaturation (field  $h$  in the context of Ising model—see the precise definition in the following section) can be obtained from the known interfacial tension. Direct Monte Carlo simulations of nucleation are also possible in this region [13–18], and transfer-matrix studies are available [19,20]. It appears that dedicated simulations support the nonclassical values of the power index of the preexponential, at least in restricted domains of temperatures [13,15,16,18,21], although in view of the limited accuracy of simulations, and of the systematic drift of the power index with temperature, the question remains partly open [18].

In the low-temperature region, the anisotropy of a system becomes crucial. In principle, in the limit  $h \rightarrow 0$ , the barrier  $W_*$  can be evaluated from the Wulff droplet construction [22–25] since the anisotropic interfacial tension can be deduced (in the two-dimensional case) from the Onsager solution. However, in view of the aforementioned limited span in the ratios  $W_*/T$  where nucleation can be actually observed, more relevant to the problem is the barrier at *finite*  $h$ . Here, exact values of  $W_*$  at  $T \rightarrow 0$  (and thus, the exponential part of the nucleation rate) were obtained by Neves and Schonmann [26]. Direct dynamic Monte Carlo simulations for the long lifetimes at low temperatures and fields are impractical due to divergence of  $I^{-1}$ . However, using the technique of Monte Carlo with absorbing Markov chains in sufficiently

strong fields [27,28,29], it is possible to obtain these long lifetimes without changing the dynamics. Alternatively, a generalized Becker-Döring approach combined with symbolic computations [30] can be employed to obtain asymptotic expansions for  $I$  at small temperatures.

At strong fields and  $T=0$ , the preexponential was first considered by Novotny [27] for Glauber spin-flip dynamics. Results pointed towards a discontinuity at  $h=1/2$ , in present notations. Subsequently, similar discontinuities were predicted for smaller  $h_m=1/2m$  (with any integer  $m$ ) in case of Metropolis dynamics [31], although a certain adjustment of the actual values of the prefactor was suggested later [32].

In Ref. [30], the case of  $T>0$  was considered for a somewhat different, “lattice-gas” dynamics which is also of non-conserved type. It was observed that the preexponential of  $I^{-1}$  develops sharp peaks in place of discontinuities. Asymptotically, for small  $T$ , each peak is described by a scaling function which depends on the dimensionless deviation of the field from  $h_m$ . Peaks do not vanish at  $T\rightarrow 0$ , but in that limit they become infinitely narrow or “unobservable” in experimental sense. More recently, a similar structure of the preexponential was observed using the aforementioned technique of the Monte Carlo simulations [28] for the Glauber dynamics and another dynamics which leads to a *divergent* prefactor at  $T\rightarrow 0$  was also studied using that technique [33].

Analytically, the treatment of nucleation for an arbitrarily small fixed  $h$  (and for any type of nonconserved spin-flip dynamics mentioned above) is possible at very low  $T$ , when only the lowest-energy cluster configurations contribute [32]. Peaks in the preexponential are observed already in this approximation, although their actual value can be modified by higher-energy nucleation paths even at  $T=0$ , and it is also unclear to what extent the off-peaks results will be modified by such paths at  $T>0$ .

Thus, the goal of the present study is to combine the power of analytical and symbolic computational approaches in order to obtain accurate expressions for a low-temperature nucleation rate. The Glauber and Metropolis dynamics will be considered, complementing the study of Ref. [30], and a more flexible identification of cluster configurations will allow us to broaden the region of fields.

## II. CLUSTER DYNAMICS

### A. Quasiequilibrium distributions

Let  $J$  characterize the interaction energy between two neighboring spins on a two-dimensional square lattice. For the external field, we will use the same dimensionless value  $h$  as in Ref. [30] with  $\pm 4Jh$  describing the interaction of this field with a down or up spin, respectively. For  $h>1$ , a system prepared with all spins pointing down is unstable since a single-spin flip reduces the energy. At  $1/2<h<1$ , the system is metastable, although the interface is unstable [34] since adding a neighbor to a single up spin reduces the energy. We will be mostly concerned with smaller  $h<1/2$  when nucleation is closer to conventional picture [8], and we will keep this picture in mind in qualitative discussions. Nevertheless, as long as one is not interested in postnucleation growth, the

domain of  $h\geq 1/2$  (including, albeit formally,  $h>1$ ) also will be covered by the present treatment.

Let us use

$$\delta = \exp(8Jh/T), \quad z = \exp(-4J/T) \ll 1 \quad (2)$$

to describe the temperature and the field dependences, respectively [30]. At zero field ( $\delta=1$ ), a system prepared with all spins initially down will develop an equilibrium distribution of up-spin clusters

$$f_i^{eq}(z,1) = w_i z^{P_i/2}, \quad (3)$$

with  $P_i$  being the perimeter of a cluster and  $w_i \leq 8$  its statistical weight. Formally, one can introduce a quasiequilibrium distribution for nonzero field as well

$$f_i^{eq}(z,\delta) = w_i z^{P_i/2} \delta^{s(i)}, \quad (4)$$

with  $s$  being the number of spins in a cluster. This distribution diverges for  $s \rightarrow \infty$  and has physical meaning only for clusters smaller than the critical size, defined below.

If all clusters had similar configurations, the perimeter  $P_i$  would be a function of  $s(i)$  (proportional to  $\sqrt{s}$  in the two-dimensional case considered). In that case,  $f_i^{eq}$  would have a minimum at the critical value  $s_*$ , in accord with the classical picture [8]. More generally, there are different configurations with the same  $s$ . If one uses extra variables to distinguish between such configurations, the function  $f_i^{eq}$  will have a saddle point. (A more subtle situation when several configurations compete for being the *critical one* will be discussed separately.) The energy corresponding to the critical configuration determines the barrier to nucleation,  $W_*$ . For  $T\rightarrow 0$ , the results for  $s_*$  and  $W_*$  were obtained in a mathematical study by Neves and Schonmann [26]:

$$s_* = m_*^2 + m_* + 1, \quad (5)$$

$$W_*/4J = 2m_* + 2 - 2h(m_*^2 + m_* + 1), \quad (6)$$

with

$$m_* = [1/2h], \quad (7)$$

where  $[x]$  denotes the greatest integer  $\leq x$  (note that this definition of  $[x]$  differs by 1 from the one used in Ref. [26]). A more elementary discussion of the above relations can be found, e.g., in Ref. [32]. The value of  $W_*/T$  determines the exponential part of the inverse nucleation rate at small temperatures and is shown by solid lines in Fig. 1.

### B. Master equation

Let  $\beta_{i,k}$  characterize transition rates between two classes  $i$  and  $k$ , defined in such a way that  $\beta_{i,k} dt$  [with  $s(i)=s(k)-1$ ] gives the probability of a transition in an infinitesimal time interval  $dt$ . More complex processes, which are described in terms of coagulation between clusters, can be neglected at low  $T$  [35].

Let an integer number  $0 \leq o_{i,k} \leq 8$  denote the number of interface sites of a cluster from class  $i$  where adding a spin

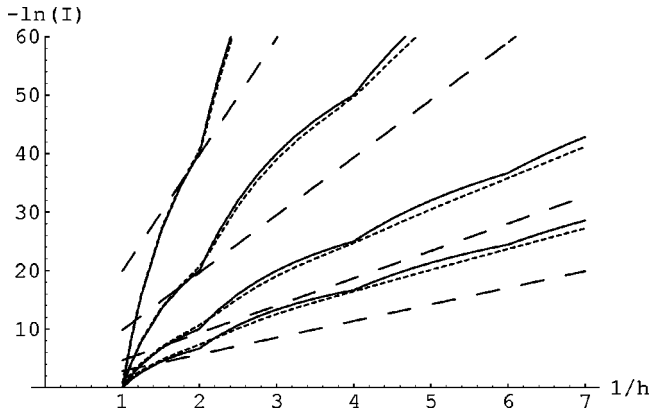


FIG. 1. Logarithm of the inverse nucleation rate as a function of field at various temperatures:  $T=0.1J$ ,  $T=0.2J$ ,  $T=0.4J$ , and  $T=0.6J$  (clockwise, short-dashed lines). The lowest-energy approximation with the Glauber dynamics was used for the plot (the present, more accurate approximation would be indistinguishable in the scale of the figure, see, however, Figs. 2 and 3 below). Values of the reduced barrier  $W_*/T$  [26] are shown by solid lines. Note that the short-dashed lines, in contrast to the solid ones, are analytic (have no cusps) at even integer  $1/h$ . The straight long-dashed lines show the reduced barriers from the droplet model for the same temperatures.

transforms it to a cluster of class  $k$ . Further, let an even integer number  $p_{ik}$  denote the change in the perimeter,  $P_k - P_i$ . Typical values of  $p_{ik}$  are 0 or 2; exceptions are  $p_{01} = 4$ , and negative values of  $p_{ik}$  when a “hole” in a cluster or a “II-shaped” depression in its surface are filled (the two latter possibilities, however, are of less interest in the context of the nucleation problem considered).

For the Glauber and Metropolis dynamics, one thus has the transition rates

$$\beta_{i,k}/o_{i,k} = \begin{cases} 1/(1+z^{-p_{ik}/2}\delta^{-1}) & \text{Glauber} \\ 1/\max(1, z^{-p_{ik}/2}\delta^{-1}) & \text{Metropolis} \end{cases} \quad (8)$$

(for the lattice-gas dynamics of Ref. [30], the rates  $\beta_{i,k}$  just coincided with  $o_{i,k}$ ).

To write down a Master equation for the kinetic distribution  $f_i$ , one can introduce fluxes

$$j_{ik} = \beta_{i,k} f_i^{eq} (v_i - v_k), \quad i < k, \quad (9)$$

with  $v_i \equiv f_i / f_i^{eq}$ . Detailed balance is satisfied automatically. One has

$$\frac{df_i}{dt} = \sum_{k=1}^{i-1} j_{ki} - \sum_{k>i}^{k_{\max}} j_{ik}. \quad (10)$$

In terms of multidimensional vectors  $\vec{f} = (f_1, f_2, \dots)$ ,  $\vec{v} = (v_1, v_2, \dots)$  and a matrix  $\hat{M}$  with elements

$$M_{ik} = \beta_{i,k} f_i^{eq} + \beta_{k,i} f_k^{eq} - \delta_{ik} f_i^{eq} \sum_{l=1}^{k_{\max}+1} \beta_{i,l} \quad (11)$$

(where  $\delta_{ik}$  is the Kronecker delta symbol), one can cast Eq. (10) as

$$\frac{d\vec{f}}{dt} = \hat{M}\vec{v} + \beta_{0,1}\vec{e}, \quad \vec{e} = (1, 0, 0, \dots). \quad (12)$$

The boundary conditions are taken as  $v_0(t) = 1$  and  $v_i(t) = 0$  for all classes  $i$  with  $s(i) = s_{up} + 1$ . The former implies that depletion of empty sites is neglected, i.e., the time scales considered are smaller than the lifetime of a metastable state and is in accord with conventional traditions [8].

The right-hand boundary conditions imply absorbing states. Similarly to conventional treatment [8], results are expected to be asymptotically insensitive to the selection of  $s_{up}$ , once it is reasonably larger than  $s_*$ . In practice, however, verification of this feature is the most challenging part of the problem since the increase of  $s_{up}$  leads to a rapid increase (faster than an exponential) in the number of configurations to be considered and thus, to the increase of the dimension of the matrix  $\hat{M}$ .

The matrix form (12) of the nucleation equation is well known in classical and near-classical descriptions—see, e.g., Ref. [36], and references therein. In particular, in the Becker-Döring case where a given class can be connected—via loss or gain of a particle—not more than to two other classes, the matrix  $\hat{M}$  has a simple tridiagonal structure and has a modest dimension of the order of  $s_{up}$ . In the present case, however, besides the aforementioned increase of dimension there is a potentially large number of connections between a given class and other classes, and the nucleation flux resembles a current through a complicated electric network [32].

### C. Nucleation rate and the preexponential

The *nucleation rate* can be defined as the total flux at a given size  $s$

$$I = \sum_{i,k} j_{ik}. \quad (13)$$

The summation is over  $i$  and  $k$  with  $s(i) = s$  and  $s(k) = s + 1$ .

In the steady-state nucleation picture considered, the above result should be insensitive to the selection of  $s < s_{up}$ . From the conventional Becker-Döring nucleation picture where an explicit transient solution is available [37], one expects that there is a sufficiently broad time interval after the end of transient effects and before depletion of empty sites or coagulation between clusters becomes important. Within such an interval, the steady-state description is valid, but the question of transient effects for Eq. (12) remains open (and in typical Monte Carlo simulations of Ising model, the interval for the steady-state nucleation can be rather short [17]).

The steady-state solution of Eq. (12) is given by

$$\vec{v} = -\beta_{0,1}\hat{M}^{-1}\vec{e}. \quad (14)$$

Since  $I$  in Eq. (13) in steady state is insensitive to  $s$ , the easiest way for its evaluation is at small  $s$  where there is no branching of nucleation path. At  $s=1$ , one has

$$I = \beta_{0,1}^2 (\hat{M}^{-1})_{11} + \beta_{0,1}. \quad (15)$$

This generalizes a similar expression [30] obtained for a different, lattice-gas spin-flip dynamics with  $\beta_{0,1}=1$ .

The inverse of the nucleation rate can be written as

$$I^{-1} = A \exp\{W_*/T\}, \quad (16)$$

with  $W_*$  being the *barrier* and  $A$  the *preexponential*. Obviously, the separation into  $W_*$  and  $A$  is not unique. As in Ref. [30], we will use for  $W_*$  its value at  $T=0$ , Eq. (6) above, which uniquely defines  $A$ . Extra argumentation in favor of this definition of  $A$  will be given in Sec. VI. Formally, the barrier will be defined as zero in the unstable region  $h>1$  (in which case the nucleation rate becomes just a rate with which spins overturn). Thus, after  $I$  is found and with definition (2), the preexponential can be obtained as

$$A = z^{W_*/4J}/I. \quad (17)$$

#### D. Realization of the approach

Evaluating the nucleation rate from Eq. (15) involves two major tasks. First, for every  $s \leq s_{up}$  one needs to obtain all relevant cluster configurations, evaluating for each class  $i$  the perimeter  $P_i$  and the weight  $w_i$ , and evaluating for each pair of classes  $i,k$  which can be connected by a single-spin flip the geometric factor  $o_{i,k}$ . A PASCAL program was written for this purpose. Since this stage is insensitive to dynamics, correctness of the cluster counting algorithm could be tested against earlier results [30] which used a somewhat different approach (see below), and for  $s_{up} \leq 5$  the numbers of distinct cluster configurations could be tested against standard tables—see the Appendix of Ref. [38]. Second, these “raw” data were used to construct the quasiequilibrium distributions  $f_i^{eq}$  and the transition rates  $\beta_{i,k}$ , thus obtaining the matrix  $\hat{M}$  for a specified dynamics. Symbolic computations using the MATHEMATICA program were employed for that purpose. In a general case, after inversion of the matrix  $\hat{M}$ , the nucleation rate  $I$  in Eq. (15) is expressed in terms of a rational function of  $z$  and  $\delta$ , although in most situations this function will be too large for a human to view. Thus, when possible, further low-temperature expansions were obtained symbolically (and this usually represented the most computationally intense part of the study) or otherwise Eq. (15) was evaluated numerically.

### III. LOW-ENERGY APPROXIMATIONS

The total number of cluster configurations grows with  $s_{up}$  faster than an exponential. Thus, if all configurations with  $s \leq s_{up}$  are taken into account, it is hardly possible to describe fields smaller, say, than  $1/4$ . On the other hand, at lower temperatures one does not expect the higher-energy configurations to have any significant contribution. This leads to the idea of *pruning* the nucleation path, by eliminat-

ing all cluster configurations which are distanced in energy by more than a few  $J$  from the most compact configurations with a given  $s$ . This reduces the dimensions of the matrix  $\hat{M}$  and makes it more sparse, simplifying the computations.

The nucleation path which involves only the most compact cluster configurations will determine the small-temperature limit (although the situation is less simple near integer  $1/2h$ ). For a given number of spins  $s$ , energies of individual clusters can change in discrete values,  $4J$ . A compact cluster is either a  $m \times m$  square, with  $m = \lfloor \sqrt{s} \rfloor$ , with possibly one extra spin on the side for  $s > m^2$ , or a  $m \times (m+1)$  rectangle, with an extra spin for  $s > m \times (m+1)$ . Energies of such clusters can be easily obtained [32].

We will be discussing two types of the lowest-energy approximations (LEA), the computer (CLEA) and the analytical (ALEA) one, respectively. The former includes all compact cluster configurations with  $s \leq s_{up}$ , and symbolic evaluation of the result in CLEA is required in a general case. Many of those compact configurations, however, will not contribute at small  $T$  and can be dropped, allowing for an ALEA which is explicitly insensitive to  $s_{up}$  [32]. The ALEA can be further improved by “dressing” the bare nucleation path with more cluster configurations, serving as a starting point for more accurate expressions.

Following Ref. [30], we will use an integer number  $\Gamma$ , the “pruning parameter,” to indicate how much higher (in units of  $4J$ ) the energy of a cluster must be compared to the energy of a compact configuration with the same  $s$ , in order for that cluster to be included in the nucleation path. In the present realization, only relevant configurations for a selected  $\Gamma$  were included from the start. (This substantially accelerated the computational speed compared to Ref. [30], where all configurations were identified initially and where pruning of the nucleation path was used on the second stage, when applying the MATHEMATICA program.) In addition, for selected runs individual configurations could be added on the cluster counting stage in order to further dress a given path, improving the accuracy and probing the potential importance of higher-energy contributions.

With finite computational resources, larger  $\Gamma$  require smaller  $s_{up}$ . In simulation, we were able to use  $s_{up} = 31$  for  $\Gamma = 0$  (the CLEA, used mostly for identification with analytics),  $s_{up} = 19$  for  $\Gamma = 1$ , and  $s_{up} = 12$  for  $\Gamma = 2$ . Note that the exact expression for  $I$  will be extremely sensitive to a selected pair of  $s_{up}$  and  $\Gamma$ . On the other hand, the asymptotic dependence (or numerical values) of  $I$  should not be sensitive to the above selection, once it is done properly.

#### A. The lowest-energy path ( $\Gamma=0$ )

Since most of the compact configurations are degenerate, there is branching of the nucleation path even in this approximation, and without further simplifications (see below), the nucleation rate can be obtained only symbolically and for a finite  $s_{up}$ . For a selected value of  $s_{up}$ , this approximation provides the *lower bound* for the steady-state nucleation rate and thus, the *upper bound* for the preexponential. In addition, as long as the temperature remains sufficiently low and since  $s_{up}$  can be reasonably large ( $s_{up} = 31$  in this case), one

expects the CLEA to be consistent with the bare analytical approximation, which can be written for  $s_{up} \rightarrow \infty$ . This provides an additional verification. Simplification of the lowest-energy treatment is possible if one removes configurations whose relative contribution is small as  $z \rightarrow 0$  and if one replaces the branching parts of the nucleation path by straight segments with equivalent contributions. Technical details are discussed in Ref. [32]. The result can be written as

$$A^{bare}(h, T) \approx z^{W_* / 4J} \left\{ \sum_{m=2}^{\infty} [g(m) + g(m-1)z\delta^m] \times z^{-2m-2} \delta^{-m^2-m-1} + \Delta \right\}. \quad (18)$$

For the Metropolis dynamics, the expansion coefficients are given by

$$g^M(m) = 3/(8m+4). \quad (19)$$

The same values can be used for the Glauber dynamics near  $T=0$ , with a slight renormalization at a higher temperature [32]. The main difference between the two dynamics comes from the  $\Delta$  terms. One has

$$\Delta^G \approx 1 + \frac{5}{4z^2\delta} + \frac{3}{8z^3\delta^2} + \frac{3}{8z^4\delta^3} \quad (20)$$

and

$$\Delta^M = \max\left(1, \frac{1}{u^2\delta}\right) + \max\left(1, \frac{1}{u\delta}\right) \left(\frac{1}{4u^2\delta} + \frac{1}{8u^3\delta^2}\right) + \frac{1}{4u^4\delta^3}. \quad (21)$$

The limit  $T \rightarrow 0$  for nonspecial values of field is determined by the dominant term in Eq. (18). One has  $A_0(1 > h > 1/2) = 5/4$ ,  $A_0(1/2 > h > 1/4) = 3/8$  (which is consistent with Ref. [27]), and  $A_0(h > 1) = 1$ . For smaller, nonspecial  $h$ , the dominant term in Eq. (18) corresponds to  $m = m_*$ , and the preexponential is given by [32]

$$A_0(h) = \frac{3}{8m_* + 4}, \quad m_* \geq 2. \quad (22)$$

The “bare” index is dropped since this result will not be affected by higher-energy paths. Similarly, the Glauber and Metropolis dynamics do not have to be distinguished at this point.

This is not the case, however, at integer  $1/2h$  where the preexponential  $A_0^{bare}(h)$  has sharp peaks which are further reduced by the higher-energy paths (as described in the following section) and which for  $h \geq 1/2$  are not identical in the Glauber and the Metropolis cases. For both dynamics, one has for  $A_0^{bare}(h_m)$  with  $h_m = 1/2m$  [32]

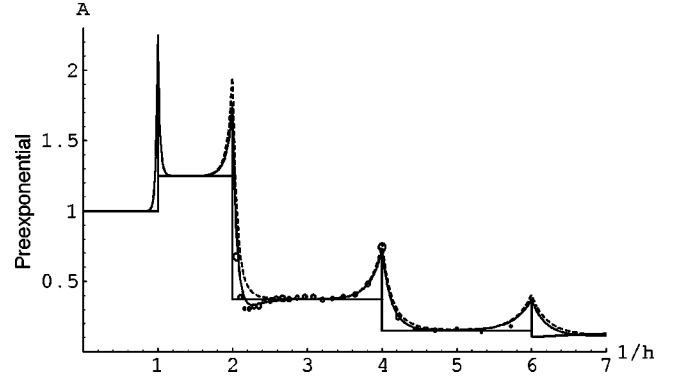


FIG. 2. The Glauber dynamics. The preexponential at  $T=0$  [linear segments] and at small  $T=0.2J$  [curves: dashed—the lowest-energy approximation of Ref. [32], Eq. (18), solid—with higher-energy corrections, Eq. (25)]. The zero- $T$  values for  $1 > h > 1/2$  ( $A_0 = 5/4$ ) and for  $1/2 > h > 1/4$  ( $A_0 = 3/8$ ) are the same as in Ref. [27]; for smaller, arbitrary  $h$ ,  $A_0$  is given by Eq. (22). “Bubbles” are the simulation data from Ref. [28] with size determined by reported errorbars multiplied, respectively, by 2 at  $h \geq 1/4$  or by 4 at  $h < 1/4$  for clarity of the figure.

$$A_0^{bare}(h_m) = \frac{3}{4} \frac{(6m+1)}{(4m^2-1)}, \quad m = 3, 4, \dots, \quad (23)$$

and  $A_0^{bare}(1/4) = 31/40$ . At  $h = 1/2$ , one has  $A_0^{bare} = 2$  and  $A_0^{bare} = 13/8$  for the Glauber and the Metropolis dynamics, respectively. When higher-energy paths are included, only the Glauber peak at  $h = 1$  ( $A_0^G = 9/4$ ) remains unchanged since there are no higher-energy configurations for a single-spin cluster (and there is no peak at  $h = 1$  in the Metropolis dynamics).

The zero-temperature preexponential for the Glauber dynamics is shown by straight line segments in Fig. 2. For the vertical segments at  $1/h = 2, 4$ , and  $6$ , the corrected renormalized values (see the following section) are used. Corresponding simulation data of Ref. [29] (not shown in the figure) are close within the reported limits of accuracy. At higher temperatures, the preexponential has a characteristic peaklike structure (dashed line in Fig. 2), similar to Ref. [30]. Qualitatively, the structure of the preexponential is mostly reproduced by the lowest-energy approximations Eq. (18). The higher-energy paths are nevertheless important to account for some subtle effects, such as the renormalization of peaks or lowering the preexponential below the zero-temperature limit near  $1/h = 2$ , similarly to non-Glauber dynamics of Ref. [30]. An account for such paths is also required for a close numerical correspondence with simulations data of Ref. [28], which are shown by bubbles in Fig. 2.

## B. Higher-energy contributions

Since the number of configurations rapidly increases with the value of  $\Gamma$ , it is impossible to treat analytically even the case  $\Gamma = 1$  for a sufficiently large value of  $s_{up}$ . (In the case of lattice-gas dynamics [30], we were able to consider  $\Gamma$

$=1$  with  $s_{up}=9$ , but the Glauber, and especially the Metropolis dynamics are more computationally demanding, and even these values represent a serious challenge for the current version of MATHEMATICA). Thus, instead of adding all configurations with higher energies to the lowest-energy path, we considered extra configurations for only selected  $s$ , which are expected to provide a significant part of the correction in a given domain of field. More specifically, for a given value of  $s_* = m_*^2 + m + 1$ , the closest square  $s = (m_* + 1)^2$  was added. The difference between  $I^{-1}$  from the computer lowest-energy approximation (with some large  $s_{up}$ ) and the one from the enriched nucleation path was evaluated symbolically and written in terms of a scaling variable [30]

$$y_n = \delta z^{1/n} \quad (24)$$

in the vicinity of a corresponding peak. Peaks are numbered starting from the one at  $h=1/2$  ( $n=1$ ), etc., and the peak near  $h=1$  is not modified by higher-energy paths and is thus excluded. We label, respectively,  $r_1(z, y_1)$ ,  $r_2(z, y_2)$ , and  $r_3(z, y_3)$ , the differences arising from adding the first excited configurations ( $\Gamma=1$ ) of the 4-, 9-, and 16-spin clusters.

Further, an expansion in fractional powers of  $z$  was obtained for each of the differences. The values of  $s_{up}$  were increased until the expansion coefficients of interest were not affected any more. Expansions were truncated on terms with relative magnitude  $O(z)$  (since many of the neglected trajectories will have a comparable contribution). The resulting differences  $r_1(z, y_1)$ ,  $r_2(z, y_2)$ , etc. were then subtracted from the bare analytical approximation to give, after multiplication by  $z^{W_*/4J}$ , the preexponential from a partly dressed nucleation path:

$$A(z, \delta) \approx A^{bare}(z, \delta) - z^{W_*/4J} \{r_1(z, y_1) + r_2(z, y_2) + r_3(z, y_3)\}. \quad (25)$$

One can check that for small  $T$  each of the corrections affects only its own peak [e.g.,  $r_1(z, y_1)$  contributes near  $h=1/2$  but will have negligible contributions near  $h=1/4$  or  $h=1/6$ ], which justifies their additive inclusion.

For the Glauber dynamics, the corrections are given by

$$r_1(z, y) = \frac{72 + 309y + 399y^2 + 179y^3 + 21y^4}{8y^2 T_1(y) z} + O(1), \quad (26)$$

with

$$T_1(y) = 6 + 64y + 190y^2 + 197y^3 + 63y^4, \quad (27)$$

$$r_2(z, y) = \frac{63}{20y^5 T_2(y) z^{5/2}} + \frac{3(6300 + 28890y^2 + 38151y^4 + 7154y^6)}{200y^8 T_2^2(y) z^2} + O(z^{-3/2}), \quad (28)$$

with

$$T_2(y) = 15 + 56y^2 \quad (29)$$

and

$$r_3(z, y) \approx \frac{0.302}{y^{10} T_3(y) z^{11/3}} + \frac{5.358 + 34.793y^3 + 84.213y^6 + 99.811y^9 + 61.905y^{12} + 8.485y^{15}}{y^{18} T_3^3(y) z^3} + O(z^{-7/3}), \quad (30)$$

with

$$T_3(y) \approx 2.195 + 6.772y^3. \quad (31)$$

At  $T \rightarrow 0$ , one has the renormalized peak values  $A_0(1/2) = 2 - 49/208 \approx 1.764$ ,  $A_0(1/4) = 0.775 - 0.0444 \approx 0.731$ , and  $A_0(1/6) \approx 0.407 - 0.0337 \approx 0.373$ . Note that the relative correction at  $T=0$  is the strongest at  $h=1/2$ , although the higher-order peaks are more sensitive to temperature.

The treatment can seem more restrictive compared to Ref. [30], where a fully dressed nucleation path was considered for  $\Gamma=1$ , but the current version has an advantage of having a result which is independent of  $s_{up}$ . [Strictly speaking, we were able to achieve this only for  $r_1(z, y_1)$  and  $r_2(z, y_2)$ ;  $r_3(z, y_3)$  is written for the maximum attainable value of  $s_{up} = 25$ .] The fully dressed path were also considered numeri-

cally for  $\Gamma=1$  ( $s_{up}=19$ ) and  $\Gamma=2$  ( $s_{up}=12$ ). Numerical results indeed are very close to Eq. (25) at lower temperatures (and would be hard to distinguish from the dashed line in Fig. 2). Even at higher temperatures, numerical and analytical results are still close in stronger fields—see Fig. 3(a) and 3(b), and the accuracy is substantially improved compared to the lowest-energy approximation, Eq. (18) (upper short-dashed line). At weaker fields, numerical results are somewhat lower than analytical results and they also slightly differ from each other, indicating the increasing role of higher-energy configurations (the  $\Gamma=2$  case can be also affected by the closeness of the absorbing boundary).

At  $T=0.4J$  both analytical and numerical predictions are close to simulation data of Ref. [28]—the bubbles in the interval  $2 < 1/h < 6$  in Fig. 3(a). This is not quite so at  $T=0.6J$  in stronger fields—see Fig. 3(b). Partly, this could be due to a limited simulation accuracy, but there

is also a difference in the operational definition of the preexponential  $A$ , as discussed in the following section.

The idea that perfect squares on the nucleation path are the first to be dressed by higher-energy configurations seems to work reasonably accurately at stronger fields. Here, it account for a noticeable renormalization of the peaks near  $h = 1/2$  [compare with the unrenormalized short-dashed value in Fig. 3(a)] and for the minor renormalization of the peak at  $h = 1/4$ . Accuracy is somewhat less at  $h = 1/6$  and  $T = 0.6J$  [Fig. 3(b)]. This could have the following explanation. When the higher-energy configurations are added to the  $2 \times 2$  square, they bring to life other dormant compact configurations which are not connected either from above or from below to another lowest-energy configuration (e.g., the *minus*-shaped 3-spin configuration, which has the same energy as the *L*-shaped one, but which cannot become a square). In the  $2 \times 2$  case this seems to be exhaustive, since all (or practically all) such extra possibilities are included. The limit  $T \rightarrow 0$  near  $h = 1/2$ , which is affected by such extra configurations, is properly reproduced. On the other hand, for smaller  $h$  the critical size is larger and is more separated from the closest square. Here, the situation with extra configurations is very rich, and it could be hard to prove that other configurations have a negligible contribution.

#### IV. METROPOLIS DYNAMICS

As mentioned, the Metropolis dynamics is computationally more intense, and we were unable to treat fields below  $h \lesssim 1/4$ . At the same time, at small fields no significant deviation from the Glauber dynamics is expected. The interesting region is related to *large* fields,  $h \gtrsim 1/2$ , where the two dynamics differ not only quantitatively but also qualitatively since there is no peak in the Metropolis dynamics at  $h = 1$ . In addition, only in this region nonanalytic properties of Metropolis transition rates become important. The latter means that the analytical structure of the nucleation peak near  $h = 1/2$  will be different for  $h > 1/2$  and  $h < 1/2$ .

In order to obtain explicit expressions for the preexponential, we used Eq. (25) with the Glauber term  $r_1(z, y_1)$  replaced by two different Metropolis terms  $R^\pm(z, y_1)$  below and above  $h = 1/2$ :

$$A^M(z, \delta) \approx A^{bare}(z, \delta) - z^{W_{*}/4J} \{R^\pm(z, y_1) + r_2(z, y_2)\}. \quad (32)$$

The term  $r_2(z, y_2)$  remained unchanged, while the term

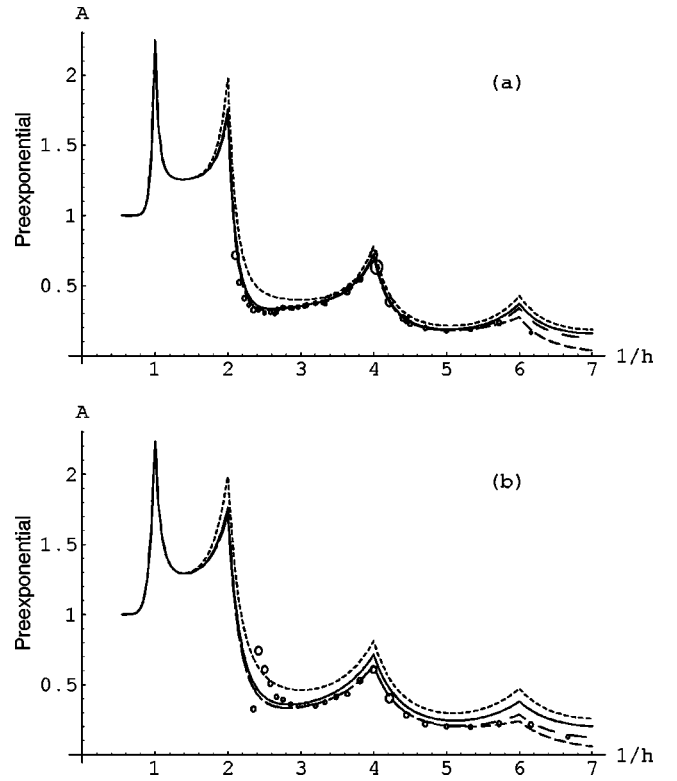


FIG. 3. The preexponential at  $T = 0.4J$  (a) and  $T = 0.6J$  (b) for the Glauber dynamics. The upper short-dashed lines are from Eq. (18), the lowest-energy approximation (upper bounds for the preexponential). Solid lines—from Eq. (25) with higher-energy corrections. Bubbles—simulation data from Ref. [28] with sizes adjusted as in Fig. 2. The two lower dashed lines are numerical results for a larger number of configurations, as described in the text. (These two dashed lines blend in with each other for  $1/h \leq 5$  and (a) also blend with the solid curve.)

$r_3(z, y_3)$  is dropped since it does not contribute in the region of fields, we are able to consider in comparative numerical studies. In addition, we kept more terms in the temperature expansions of  $R^\pm$  to emphasize that at strong fields nearly all relevant configurations are taken into account and not only the most compact ones. [Strictly speaking, “coagulation paths” or disconnected cluster configurations—see the following section—can give a relative contribution of  $O(z)$ , but those effects are beyond the current treatment.] The results for  $R^\pm$  are given by

$$R^+(z, y) = r_1(z, y) + \frac{432 + 5076y + 23\,952y^2 + 58\,639y^3 + 80\,266y^4 + 61\,504y^5 + 24\,498y^6 + 3933y^7}{8y^3T_1^2(y)} + \frac{(18 + 71y + 81y^2 + 27y^3)(6 + 28y + 43y^2 + 27y^3 + 6y^4)^2}{8y^4T_1^3(y)} z + O(z^2), \quad y < 1, \quad (33)$$

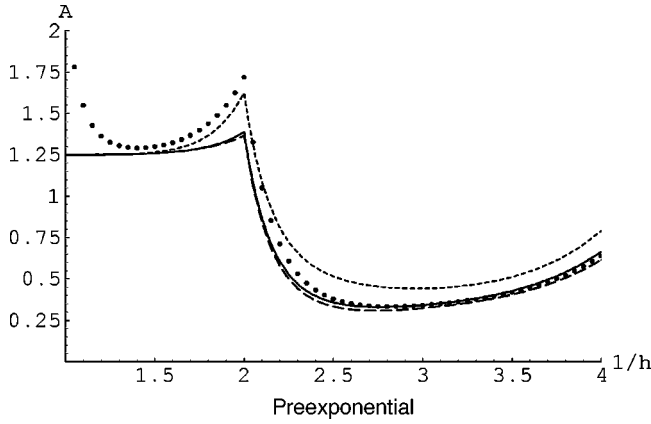


FIG. 4. The preexponential near  $h=1/2$  for the Metropolis dynamics at  $T=0.6J$ . Upper short-dashed line—the bare, lowest-energy path approximation. Solid line—the bare path “dressed” with excited configurations of a 4-spin cluster. Lower dashed line—numerical results (which also include a large number of other excited configurations—see text). For comparison, numerical data for the Glauber dynamics are indicated by points. Note that the latter dynamics leads to a peak at  $h=1$  which is absent in the Metropolis case and a higher peak at  $h=1/2$ , but for smaller  $h$  predictions of the two dynamics practically blend with each other.

with  $r_1(z, y)$  and  $T_1(y)$  the same as for the Glauber dynamics, and

$$R^-(z, y) = \frac{77 + 168y}{4y^2 V(y)z} + \frac{3(610 + 4307y + 9696y^2 + 6912y^3)}{8y^4 V^2(y)} + \frac{25(3 + 8y)^2(53 + 144y)}{16y^6 V^3(y)} z + O(z^2), \quad y > 1, \quad (34)$$

with

$$V(y) = 15 + 101y + 144y^2. \quad (35)$$

The renormalized value of the  $h=1/2$  peak at  $T=0$  is  $13/8 - 49/208 \approx 1.389$ . The absolute value of the correction is identical to Glaubers, although the relative effect is stronger in the Metropolis case. The results of comparison with numerical studies obtained for  $\Gamma=1$  and  $s_{up}=9$  at  $T=0.6J$  are shown in Fig. 4. Note the closeness of predictions from the Metropolis dynamics (lines) and Glauber dynamics (points) at fields smaller than  $h \approx 1/3$ , although at stronger fields the difference is quite noticeable. The bare analytical approximation—upper short-dashed line in Fig. 4—is qualitatively reasonable, but it overestimates the peak near  $h=1/2$  (correspondence here with the full, numerical predictions for the Glauber dynamics is coincidental). With the higher-energy corrections included, Eq. (32)—solid line in Fig. 4—there is virtually no difference between the analytical and numerical results, despite the relatively high temperature considered.

## V. DOMAINS OF VALIDITY OF THE RESULTS AND POTENTIAL APPLICATIONS

The above treatment was based on selecting a large number of cluster configurations (and various approximations differ in specifics of such selection) and writing down a master equation (ME) describing the intercluster kinetics. In practice, our ability to solve the ME is currently limited by the size of the matrix which is to be inverted, or, equivalently, by the number of cluster configurations considered. Thus, strictly speaking, the results are restricted to lower temperatures and moderately strong fields. The former allows one to rely on the lowest-energy nucleation path, adding only a selected number of higher-energy configurations in order to improve the accuracy. Larger  $h$ , on the other hand, restrict the number of spins  $s$  in clusters to be included due to reduction of the critical number  $s_*$  with the possibility to lower the upper boundary  $s_{up}$ .

Operationally, adequacy of the temperature domain is tested by including additional higher-energy configurations and verifying that there is no substantial change in the results. Since, away from  $T=0$ , the temperature dependence of the preexponential is exceptionally modest, temperatures up to  $0.6J \approx 0.26T_c$ —see Fig. 3, can be considered. A crude estimation of the temperature domain where the lowest-energy approximation is valid can be obtained from the condition that for clusters with  $s = m_*^2$  spins, the single compact configuration (the square) has a dominant contribution compared to the contributions from excited configurations. Energies of the first excited configurations exceed the energy of the square by  $4J$ , and the number of such configurations, approximately increases as  $s^2$  [39]. This gives

$$T \lesssim J / [-\ln(2h)]. \quad (36)$$

The latter condition was satisfied for all fields and temperatures considered, resulting in only moderate effects of higher-energy contributions.

The field domain is adequate as long as the critical number is noticeably smaller than  $s_{up}$ . However, the exact verification of the insensitivity to  $s_{up}$  is much more challenging compared to the conventional case [8] and the required distance between  $s_*$  and  $s_{up}$  can be much larger. Indeed, consider, for example a “precritical” cluster which has a shape of a  $m_* \times (m_* + 1)$  rectangle (with  $m_*^2 + m_* + 1$  determining the critical cluster number). Turning this cluster into critical requires adding a spin to the *longer* side of the rectangle. However, there is also a “blind alley” to nucleation, namely, adding a spin to the shorter side. If the distance between the absorbing boundary and  $s_*$  is smaller than  $m_* - 1$ , this alley will, incorrectly, lead to a successful nucleation event, overestimating the nucleation rate. Thus, for small  $h$ , one requires at least  $s_{up} - s_* \gtrsim (s_*)^{1/2}$  as  $T \rightarrow 0$ . In this context, results which include symbolic computations are reliable for  $h \gtrsim 1/4$ . At higher  $T$ , there is an additional requirement that energies of other “extremal” [32] configurations along the nucleation path also should be included if they are sufficiently close to  $W_*$ . Energies of the most important of such configurations (“primary configurations” in terms of Ref.

[32]) are given by Eq. (6) with  $m_*$  replaced by an integer number  $m$ . This gives  $m - m_* \gtrsim \sqrt{T/2h}$ , with  $s_{up} > m^2 + m + 1$  (the latter condition was satisfied in the present study, but should be kept in mind for smaller  $h$ ).

Note that the above restrictions are mostly of technical nature, and more advanced computer power (as well as more dedicated algorithms, tailored to the specific structure of the ME) would allow one to include more configurations, potentially expanding the domains of  $T$  and  $h$ . There are several limitations, however, which are related to the ME itself, which ignores the cluster-cluster interactions.

In the present case, similarly to conventional nucleation description [8], only transitions between clusters with neighboring sizes are considered. Coagulation effects (and the reverse breaking of clusters in two parts) are ignored, again restricting the temperature. Intuitively, such effects should not be important for small  $T$ , although a precise quantification of the temperature domain where they can be ignored is beyond the scope of the present study. In principle, it would be possible to include directly such effects in the proposed scheme by generalizing the definition of a “cluster,” allowing clusters consisting of close disconnected configurations, which can be connected by a single-spin flip. The actual realization of this program extends, however, beyond the current work.

There is also an implicit restriction of the field from above since for large  $h$  and  $T > 0$  the lifetime of a metastable state will be too short, comparable to the duration of transient nucleation effects, and there will be no steady-state nucleation regime. Transient nucleation effects can be directly deduced from the above ME, although this will require a separate study. The lifetime of metastable state, on the other hand, can depend on cluster-cluster coagulation or at least on the depletion effects, leading to a modification of the left-hand boundary condition  $v_0 < 1$  which is beyond the current version of the ME.

When comparing the results with those from Monte Carlo with absorbing Markov chains simulations [28], one should keep in mind the difference in interpretation. Reference [28], and earlier works of this direction, considers the *lifetime of a metastable state*  $\tau$ —in practice, the time when magnetization achieves a predetermined value. This time, obviously, depends on the system size [15]. On the other hand, the nucleation rate  $I$  described in the present study has no dependence on system size although the latter determines the experimental interpretation [17]. If  $L^2$  is the number of spins in a system and this number is large enough for many nuclei to be formed, then  $L^2 I$  is just the rate with which nuclei are added to the system. Both in real experiments [3] or in simulations with the Ising system [17], the steady-state nucleation rate  $I$  can thus be measured from the slope of the number of larger-than-critical nuclei as a function of time. Alternatively, if  $L^2 I$  is small, only a single nucleus is formed (it is still assumed that the system is large enough for the boundary conditions to have no special effect on the nucleation rate). The subsequent growth of this nucleus completes the phase transition. In this case,  $1/L^2 I$  is the average waiting time for this nucleus to appear (again, neglecting the transient nucleation effects); and this waiting time is most closely related to the

lifetime of a metastable state. In fact,  $1/I$  is expected to be identical to  $\tau$  for small systems, once the lifetime is multiplied by the number of spin, as in Ref. [28]. At low temperatures, any finite system becomes “small,” and a close correspondence between the obtained analytical expansions for  $I^{-1}$  and simulation data for  $\tau$  of Ref. [28] is observed—see Figs. 2 and 3(a). For higher temperatures, however, such a simple correspondence between  $\tau$  and  $1/I$  does not exist, which might be (partly) responsible for the differences in Fig. 3(b).

Finally, potential application of the obtained results should be mentioned. Direct Monte Carlo simulations of phase transitions in the Ising model [14,15,17,18,21] usually do not go lower than  $0.5 - 0.6T_c$ , and temperatures of  $0.8T_c$ , and higher, are quite common. The reason for this is the aforementioned rapid drop in the nucleation rate at smaller  $T$ , which makes the waiting time for even a single nucleus to appear too long on the scale of the computational experiment. However, although the higher-temperature nucleation bears many visual and semiquantitative similarities with the conventional nucleation picture [8], many fine issues are blurred by the closeness to  $T_c$  (for example, it is unclear to which extent interaction between nuclei can be neglected [18]). Moreover, many experiments on two-dimensional systems, e.g., Ref. [40] (for which the Ising model seems to be most relevant) deal with temperatures well below  $T_c$  [25]; simulations of growth for such cold systems also reveal many interesting features [34]. One of the possibilities to bypass the direct simulations of the nucleation process and bridge the disperse time scales is to combine the Monte Carlo approach with the technique of absorbing Markov chains, as used for simulations of magnetization switching in micromagnetic materials [6]. Alternatively, the obtained results, which provide analytical expressions for the nucleation rate  $I$ , can be used in low-temperature simulations with nucleation described as a random Poissonian generation of nuclei, with the average time separating the random events given by  $1/L^2 I$ . Growth of nuclei, which requires much smaller time scales, can then be simulated in a conventional way [34]. Transient nucleation effects, which are non-Poissonian [17], can be further included once corresponding expressions for  $I(t)$  are obtained.

## VI. DISCUSSION

In the present work, we obtain several analytical and numerical approximations for the steady-state nucleation rate  $I$  in the metastable Ising model driven by the Glauber or by the Metropolis dynamics.

The treatment generalizes the results of Ref. [30] which were obtained for a different dynamics, but the current approach also adds more flexibility in selecting cluster configurations, allowing one to consider smaller fields. The presence of sharp peaks in the low-temperature preexponential of the nucleation rate appears to be a universal feature, at least for spin-flip dynamics of nonconserved type. The magnitudes of those peaks, however, are sensitive to dynamics. At smaller fields,  $h \leq 1/4$ , the Glauber and Metropolis dynamics leads to nearly identical predictions, but results differ for  $h \geq 1/2$ , and

at any field results are quantitatively different from those for the lattice-gas dynamics of Ref. [30]. Compared to Ref. [32] where the lowest-energy nucleation path was considered analytically, the present study adds the effects of higher-energy configurations which improves the accuracy at  $T > 0$  and leads to a renormalization (lowering) of the peaks in the preexponential which persists up to  $T = 0$ . The latter effect is most pronounced at  $h = 1/2$  where it exceeds 10% at  $T = 0$ . Lowering of the peak at  $h = 1/4$  is much smaller, only a few percent, although it is currently unclear to which extent this tendency will persist in weaker fields.

In separation of the inverse nucleation rate into an exponential and a preexponential factors, we followed the pattern of Ref. [30] where the known zero-temperature expression [26] for the nucleation barrier is used, while all temperature dependence is included in the prefactor. There is no special explanation for such a separation except for convenience, since the “observable” is the nucleation rate, and there always remains a certain degree of flexibility when splitting it into two factors. An additional justification comes from the fact that once defined in such a manner, in the domain of moderately strong fields considered, the preexponential indeed is only weakly sensitive to temperature, in accord with conventional expectations [8]. As one can see from Figs. 2 and 3, after an initial broadening of the peaks compared to  $T = 0$ , further increase of temperature leads to very modest modifications of  $A$ , by a few percent, while the exponential term changes here by many orders of magnitude. It is still unclear, though to which extent the low-temperature expansions for the preexponential will be modified (reduced) with increased temperature at smaller fields where the contribution of higher-energy configurations becomes much more important.

One of the alternatives to the zero-temperature barrier  $W_*$  [26] would be the “droplet model” (DM) barrier  $W^{DM}$ , which uses the bulk, temperature-dependent interfacial tension. (In fact, most of the high-temperature studies mentioned in the Introduction, e.g., Refs. [11,12,19] rely on the DM barrier). Ideally, one could wish to start with a strictly discrete, low-energy construction for a nucleus, and be able to trace the transition to the DM when the nucleus gets sufficiently large (small  $h$ ) and when excited configurations are added. Hypothetically, this would take place at exponentially small  $h$ , approximately determined by condition (36). The present treatment, however, does not allow one to do that since only restricted numbers of excited configurations can be included (see also a discussion in Ref. [32]). Once the nucleation rate is obtained, however, it is possible to introduce the DM barrier formally, by including it into the expo-

nenial, and use the prefactor to comply with the calculated rate.

In a general case, the interfacial energy of a nucleus obtained in the DM via the Wulff construction can be expressed in terms of elliptic integrals [23], and elementary interpolating approximations to  $\sigma_{eff}$  at higher and lower temperatures are available [18]. At low  $T$ , the Wulff construction will be close to a perfect square (which corresponds to  $T = 0$ ) with a correction to interfacial energy which is quadratic in  $T$  [18]. This results in a difference between the barriers at small temperatures

$$W_*(h) - W^{DM}(h, T) = 4J \left[ 1 - \frac{h}{2} [3 + 4a(h)^2] + \frac{1}{h} O[(T/J)^2] \right], \quad (37)$$

with a “sawtooth” oscillatory function

$$a(h) = m_*(h) - 1/2h + 1/2, \quad |a| \leq 1/2.$$

Note that the DM barrier is identical to  $W_*$  at  $h = 1/2$  and  $T = 0$ , but at smaller fields the DM barrier is smaller, and the deviation from  $W_*$  increases with temperature. As one can see from Fig. 1, in order to comply with the low-temperature values of  $1/I$  (short-dashed lines), the exponential parts of the DM (long-dashed lines) would require prefactors which increase with  $1/h$  at small  $h$  (and which can be nonmonotonic at larger  $h$  for small  $T$ ), and which can be exponentially large. The latter does not mean necessarily that the DM barrier is “wrong” since in conventional traditions [8] a large preexponential could be consistent with a slow growth rate, but generally care should be taken when using the DM at low  $T$  where the prefactor can provide a sizable correction to the exponential term.

Thus, the question of the “best” selection of the nucleation barrier (which would strongly affect the associated preexponential) remains open, although also somewhat of academic interest. From a practical point, the main value of the study could be the full expression for the nucleation rate, which potentially can help in overcoming the large nucleation time scales encountered in low-temperature simulations of the phase transformation kinetics.

#### ACKNOWLEDGMENTS

The authors wish to thank M. A. Novotny for the high-resolution version of the figures from Ref. [28] and for useful comments on the manuscript.

- 
- [1] F.F. Abraham, *Homogeneous Nucleation Theory* (Academic Press, New York, 1974).  
 [2] P. Debenedetti, *Metastable Liquids* (Princeton, New Jersey, 1996).  
 [3] P. James, *Phys. Chem. Glasses* **15**, 95 (1974); V. Fokin, A. Kalinina, and V. Filipovich, *Fiz. Khim. Stekla* **3**, 122 (1977); J.

- Deubener, *J. Non-Cryst. Solids* **274**, 195 (2000).  
 [4] C. Spinella, S. Lombardo, and F. Priolo, *J. Appl. Phys.* **84**, 5383 (1998).  
 [5] R.M. Westerwelt, *Phys. Status Solidi B* **74**, 727 (1976); **76**, 31 (1976); I.M. Fishman, *Usp. Mat. Nauk*, **155**, 329 (1987).  
 [6] M.A. Novotny, G. Brown, and P.A. Rikvold, *J. Appl. Phys.* **91**,

- 6908 (2002).
- [7] U. Gasser, Eric R. Weeks, Andrew Schofield, P.N. Pusey, and D.A. Weitz, *Science* **292**, 258 (2001); V.J. Anderson and H.N.W. Lekkerkerker, *Nature (London)* **416**, 811 (2002).
- [8] M. Volmer and A. Weber, *Z. Phys. Chem., Stoechiom. Verwandtschaftsl.* **119**, 227 (1926); L. Farkas, *ibid.* **125**, 236 (1927); R. Becker and W. Döring, *Ann. Phys.* **24**, 719 (1935); Ya.B. Zeldovich, *Acta Physicochim. URSS* **18**, 1 (1943); J. Frenkel, *Kinetic Theory of Liquids* (Oxford University Press, Oxford, 1946).
- [9] J. Lothe and G. Pound, *J. Chem. Phys.* **36**, 2080 (1962).
- [10] H. Reiss, J.L. Katz, and E. Cohen, *J. Chem. Phys.* **48**, 5553 (1968).
- [11] M.E. Fisher, *Physics (Long Island City, N.Y.)* **3**, 255 (1967).
- [12] J.S. Langer, *Ann. Phys. (N.Y.)* **65**, 53 (1971).
- [13] E. Stoll, K. Binder, and T. Schneider, *Phys. Rev. B* **6**, 2777 (1972).
- [14] K. Binder and D. Stauffer, *Adv. Phys.* **25**, 343 (1976).
- [15] P.A. Rikvold, H. Tomita, S. Miyashita, and S.W. Sides, *Phys. Rev. E* **49**, 5080 (1994).
- [16] M.A. Novotny, P.A. Rikvold, M. Kolesik, D.M. Townsley, and R.A. Ramos, *J. Non-Cryst. Solids* **274**, 356 (2000).
- [17] V.A. Shneidman, K.A. Jackson, and K.M. Beatty, *Phys. Rev. B* **59**, 3579 (1999).
- [18] V.A. Shneidman, K.A. Jackson, and K.M. Beatty, *J. Chem. Phys.* **111**, 6932 (1999).
- [19] C.C. Günther, P.A. Rikvold, and M.A. Novotny, *Phys. Rev. Lett.* **71**, 3898 (1993); *Physica A* **212**, 194 (1994).
- [20] S.B. Rutkevich, *J. Stat. Phys.* **104**, 589 (2001).
- [21] R.A. Ramos, P.A. Rikvold, and M.A. Novotny, *Phys. Rev. B* **59**, 9053 (1999).
- [22] C. Rottman and M. Wortis, *Phys. Rev. B* **24**, 6274 (1981).
- [23] R.K.P. Zia and J.E. Avron, *Phys. Rev. B* **25**, 2042 (1982).
- [24] R.K.P. Zia, *J. Stat. Phys.* **45**, 801 (1986).
- [25] V.A. Shneidman and R.K.P. Zia, *Phys. Rev. B* **63**, 085410 (2001).
- [26] E.J. Neves and R.H. Schonmann, *Commun. Math. Phys.* **137**, 209 (1991).
- [27] M.A. Novotny, in *Computer Simulation Studies in Condensed-Matter Physics IX*, edited by D.P. Landau, K.K. Mon, and H.-B. Schüttler (Springer, Berlin, 1997), p. 182.
- [28] M.A. Novotny, in *Computer Simulation Studies in Condensed-Matter Physics XV*, edited by D.P. Landau, S.P. Lewis, and H.-B. Schüttler (Springer, Berlin, 2003), p. 7.
- [29] K. Park and M.A. Novotny, *Comput. Phys. Commun.* **147**, 737 (2002).
- [30] V.A. Shneidman and G.M. Nita, *Phys. Rev. Lett.* **89**, 025701 (2002).
- [31] A. Bovier and F. Manzo, *J. Stat. Phys.* **107**, 757 (2002).
- [32] V.A. Shneidman, *J. Stat. Phys.* **112**, 293 (2003).
- [33] K. Park, M.A. Novotny, and P.A. Rikvold, *Phys. Rev. E* **66**, 056101 (2002).
- [34] V.A. Shneidman, K.A. Jackson, and K.M. Beatty, *J. Cryst. Growth* **212**, 564 (2000).
- [35] J.P. Marchand and P.A. Martin, *Physica* **127A**, 681 (1984).
- [36] D.T. Wu, in *Solid State Physics: Advances in Research and Applications*, edited by H. Ehrenreich and F. Spaepen (Academic Press, San Diego, 1996), pp. 37–187.
- [37] V.A. Shneidman, *Zh. Tekh. Fiz.* **57**, 131 (1987) [*Sov. Phys. Tech. Phys.* **32**, 76 (1987)]; **58**, 2202 (1988) [**33**, 1338 (1988)].
- [38] C. Domb, *Adv. Phys.* **9**, 149 (1960).
- [39] V.A. Shneidman and G.M. Nita (unpublished).
- [40] G. Schulze Icking-Konert, M. Giesen, and H. Ibach, *Phys. Rev. Lett.* **83**, 3880 (1999).